applied sciences

Article

Nanosecond Breakdown Characteristics of C_4F_7N and Various Mixtures at Pressures Above 1 Atmosphere in Comparison with SF_6

Luke Silvestre [1,*], Jakob Matthies [1], Luke Boswell [1], Jacob Stephens [1], James Dickens [1], Andrew Young [2] and Andreas Neuber [1]

[1] Center for Pulsed Power and Power Electronics Research, Department of Electrical and Computer Engineering, Texas Tech University, Lubbock, TX 79409, USA
[2] Lawrence Livermore National Laboratory, Livermore, CA 94550, USA
* Correspondence: p3e@ttu.edu

Featured Application: This work measures the nanosecond pulsed breakdown performance of C_4F_7N and compares it to that of SF_6. The results indicate that C_4F_7N and its various mixtures exhibit certain advantages in breakdown behavior over simply pure SF_6 in pulsed spark gaps.

Abstract: This report evaluates the pulsed breakdown performance of C_4F_7N under a 6.8 kV/ns voltage excitation. The pulsed dielectric strength of C_4F_7N is compared to SF_6 in the same experimental setup, and it is found that C_4F_7N concentrations of 50% or greater are required to achieve a dielectric strength greater than or equal to SF_6. Pure C_4F_7N demonstrated higher electric field hold-off for longer time periods and less statistical variance under pulsed conditions when compared to SF_6. Mixtures of 50% C_4F_7N with N_2 or CO_2 as buffer gases showed no appreciable difference in pulsed dielectric strength.

Keywords: C_4F_7N; SF_6; Novec^{TM} 4710; pulsed breakdown; dielectric strength; electrical breakdown; capacitive voltage divider; Rogowski coil; insulating gas; sulfur hexaflouride

Citation: Silvestre, L.; Matthies, J.; Boswell, L.; Stephens, J.; Dickens, J.; Young, A.; Neuber, A. Nanosecond Breakdown Characteristics of C_4F_7N and Various Mixtures at Pressures Above 1 Atmosphere in Comparison with SF_6. *Appl. Sci.* **2024**, *14*, 11268. https://doi.org/10.3390/app142311268

Academic Editor: Gerard Ghibaudo

Received: 31 October 2024
Revised: 27 November 2024
Accepted: 27 November 2024
Published: 3 December 2024

1. Introduction

There has been interest in finding alternative gases to SF_6 for use in high voltage systems [1,2]. C_4F_7N has been considered as one of the alternatives to SF_6, and the appeal is two-fold [3]. First, C_4F_7N has already been demonstrated to have a dielectric strength greater than or equal to SF_6 in AC or DC electric fields, even when mixed with CO_2 at fractional concentrations of 15–20% [4–8]. Second, C_4F_7N has an atmospheric lifetime of 30 years, giving it a much lower global warming potential compared to SF_6 [9].

When not diluted with a buffer gas, C_4F_7N has a dielectric strength 2.6 times greater than SF_6, up to 1000 kPa·mm [10]. Studies on the molecular dynamics of e^- + C_4F_7N collisions have characterized effective ionization rates, excited, ionization, attachment, elastic, and effective cross sections [10–14]. When used as an insulating gas in an electrical breakdown C_4F_7N has multiple by-products that arise from these different collision types [12,14]. The chemical compatibility of C_4F_7N and its by-products must be considered in spark gap design. Ethylene propylene diene monomer (EPDM) rubbers, nitrile, and PMMA plastics have shown signs of degradation in C_4F_7N environments [15,16]. Coating these structures in silicon grease adds a protective barrier that mitigates the degradation caused by C_4F_7N, but this is an ad hoc solution [15]. Silver and aluminum are compatible with C_4F_7N, but after 40 h of exposure at 220 °C, C_4F_7N mixtures demonstrated corrosive effects on copper [17,18]. Various gas adsorbents and desiccants have also been studied for their effectiveness in C_4F_7N environments [19]. The deleterious effects of C_4F_7N are circumvented in this setup using two techniques. First, compatible materials are used

or coated in a thin layer of grease whenever possible. Second, C_4F_7N and its mixtures remain in the testing apparatus for no more than 90 min at a time and at room temperature, after which they are evacuated. This setup is designed to minimize the amount of material degradation induced by C_4F_7N.

Pulsed breakdown measurements are performed on a pressurized experimental apparatus that allows for the measurement of breakdown behavior with nanosecond temporal resolution. The C_4F_7N mixing percentages tested are 50%, 50/50, and 20%, 20/80, with a buffer gas as the remaining percentage. The buffer gases used are CO_2 and N_2. Custom voltage and current diagnostic probes were manufactured and calibrated to handle pulsed excitations with a frequency bandwidth greater than 350 MHz. An electrically triggered Marx generator is used to produce a consistent voltage pulse for statistical comparisons. The experimental apparatus is a 3.8 L chamber with pressures ranging from 101.3 kPa to 456 kPa being tested. All pressures measurements in this report are recorded as absolute pressure.

2. Experimental Setup

The pressure chamber, gray box in Figure 1, is designed for pressures up to 517 kPa. The pressure chamber is pumped down via a roughing pump to below 40 mtorr before being filled with the gas under test.

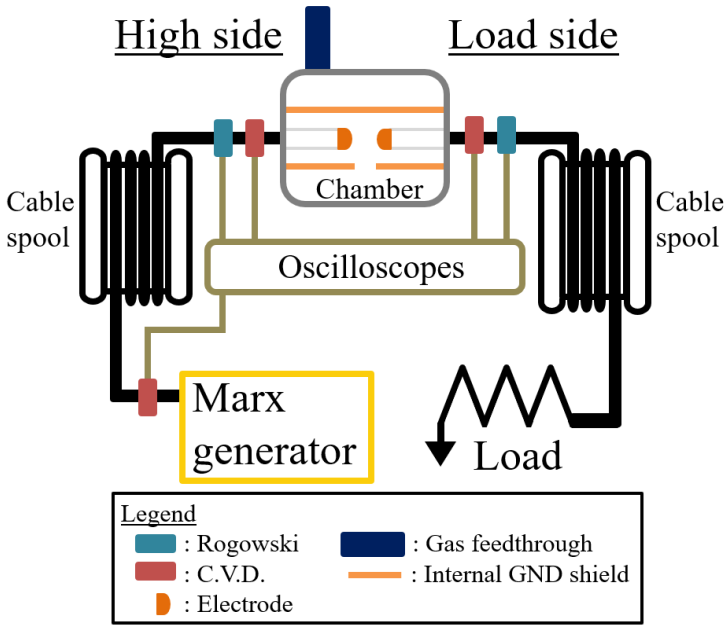

Figure 1. A pictographic representation of the spark gap test setup. The cable spools consist of 14.9 m of 2121 coaxial transmission line cable. The cables temporally isolate the spark gap from voltage reflections at the Marx generator or load. The Rogowski coils and capacitive voltage dividers, CVD, provide current and voltage diagnostics, respectively. The Marx generator is electrically triggered using a trigatron. The 2121 cable is sourced from US manufacture dielectric sciences (Chelmsford, MA, USA). The Marx generator, Rogowski coils, and CVDs are designed and fabricated the Texas Tech University Center for Pulsed Power and Power Electronics.

Inside the chamber is the spark gap with a ground shield across the gap to maintain the coaxial transmission line nature of the cable spools on either side, see Figure 1. The ground shield permits nanosecond temporal resolution across the gap. The cable spools are 2121 high voltage, HV, coaxial transmission line cables and are electrically long to temporally isolate the spark gap from source and load reflections. The one-way electrical delay of the cable spools is 85 ns. The measured impedance of the 2121 HV cable is 59 Ω. The HV pulse is dissipated using a 50 Ω resistive load. The temporal region of interest in

the measured gap voltage signal is ≈30 ns. Thus, reflections from the impedance mismatch of the 2121 HV cable and the load arrives well after the spark has finished breaking down.

On either side of the chamber are Rogowski and capacitive voltage divider, CVD, probes to measure transient current and voltage waveforms. The probes are mounted on the high and load side of the chamber; the high side is connected to the Marx generator, and the load side is connected to the load. These probes measure the nanosecond pulses across the gap if breakdown occurs. Voltage and current measurements are denoted with H or L subscripts depending on which side of the chamber they are mounted, see Figure 1. The high voltage pulse is produced using a pressurized Marx generator, which is electrically triggered. The output of the Marx generator is measured with its own CVD probe. The Marx generator is fired in 90 s intervals. To mitigate any effects of material compatibility, all insulating gases were evacuated from the system after 90 min. After the data were taken, the chamber was pumped down to below 30 mtorr and back-filled with lab air or N_2.

The gas mixtures are created by filling the chamber with partial pressures of C_4F_7N and the buffer gas. The gas mixtures tested are 50/50 C_4F_7N with N_2 or CO_2 as the buffer gas or a 20/80 C_4F_7N mixture with N_2. To create a homogeneous gas mixture, a fan at the base of the chamber is spun via magnetic coupling for ten minutes prior to testing. During this time, the mixing fan is spun at 2000 rpm or greater with an approximate gas flow rate of 337 L/min or greater.

2.1. Test Gap

The spark gap is constructed using 2 hemisphere electrodes, see Figure 2. The ground shield has 4 vent holes with a diameter of 6.3 mm spaced 90° apart around the center of the spark gap. The vent holes in the ground shield permit the gases under test to fill the spark gap while maintaining a coaxial transmission line structure across the gap. The ground shield is coated in a layer of epoxy to prevent the breakdown of the external ground shield instead of across the gap. The electrodes are mounted in PEEK sleeves, see Figure 2, to prevent breakdown from initiating at the junction between the electrode and the 2121 cable. Once the system is fully mounted, the gap distance between the electrodes is 2.2 mm.

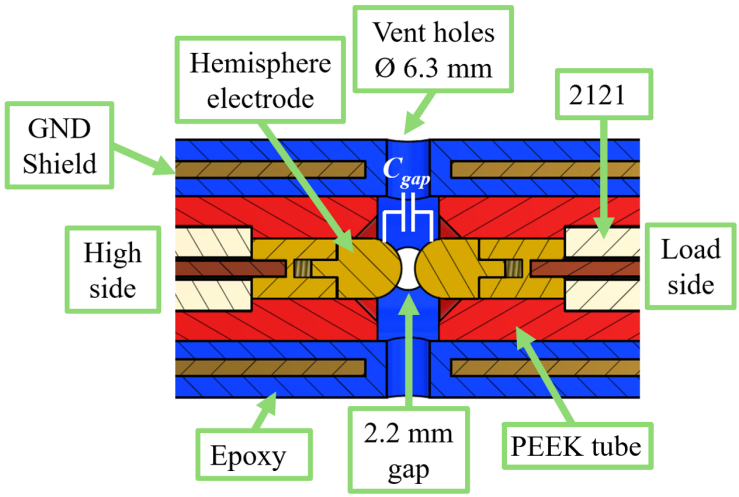

Figure 2. A cross-section view of the spark gap within the pressure chamber to scale. The gap capacitance C_{gap} was calculated to be 1.6 pF. The vent holes allow for insulating gas to fill the gap. The PEEK tubes help mitigate tracking from the junction between the electrodes and the 2121 cable. The ground shield is made from a single cylinder cut in half lengthwise. These halves are potted in epoxy to prevent breakdown to them. This cross-section does not show the ground electrically connected across the gap.

CST simulations of the spark gap calculated the capacitance across the gap, C_{gap}, to be 1.6 pF, see Figure 2. CST simulation calculated the field enchantment factor of the gap to be 1.315. Thus, the macroscopic electric field is multiplied by 1.315 to determine the peak

electric field at breakdown. The macroscopic electric field is the maximum voltage, V_{max}, prior to breakdown divided by the gap distance, d.

2.2. Electrical Diagnostics

The diagnostic probes used are coaxially mounted capacitive voltage dividers, CVD, and Rogowski probes, see Figure 3. The Rogowski coils and CVDs are designed, manufactured, and calibrated at the Texas Tech University Center for Pulsed Power and Power Electronics. These diagnostics permit the passive measurement of large amplitude voltage (10's–100's kV) and current (1 kA–100's kA) transients over a wide frequency range [20–25].

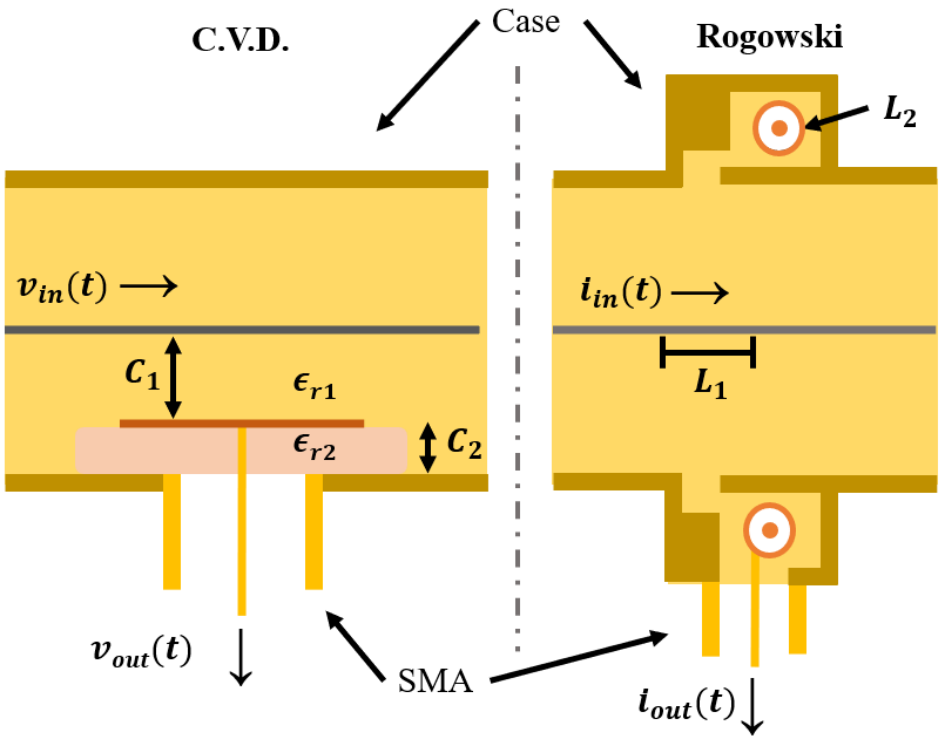

Figure 3. A cross-section representation of the CVD and Rogowski probes on the setup, not to scale. C_1 is the capacitance between the inner conductor and copper tape. Kapton tape produces the dielectric barrier for the second capacitance, C_2, between the copper and brass electrodes. L_1 is the inductance of the inner conductor, which couples to L_2 of the Rogowski coil. The Rogowski coil uses an azimuthal slit to mitigate the capacitive coupling of L_2 to L_1. The case of both probes is made out of brass.

An RF design rule of thumb stipulates that a signal 10% to 90% risetime, $\tau_{10/90}$, has a frequency bandwidth, f_{BW}, equivalent to $f_{BW} = 0.35/\tau_{10/90}$ [21]. Thus, a risetime of 1 ns requires a frequency bandwidth of 350 MHz. The CVD and Rogowski probes' transfer function, H, was measured using a vector network analyzer, VNA, and calculated using Equation (1) [23]. The CVD and Rogowski probes are calibrated on a 100-m-long spool of 2121 cable. The 2121 cable has a characteristic impedance of 59 Ω and is terminated with a matched load when used for calibration.

$$H = \frac{S_{21}}{1 - S_{11}} \quad . \tag{1}$$

The transfer function of the high-side probes is shown in Figure 4. The CVD probe follows a slope of 20 dB per decade until it levels off. The transition region of the CVD is the −3 dB point of the transfer function. Before the −3 dB point, CVD operates in a derivative mode. After the −3 dB point, the CVD is self-integrating [21]. Fourier transform signal corrections permit the CVD to have a bandwidth of 2.5 GHz, resulting in a minimum

possible resolution of 140 ps, see Figure 4. The Rogowski probe transfer function has a valley around 850 MHz, which limits the bandwidth, see Figure 4. The bandwidth used in data processing is 600 MHz, resulting in a minimum possible resolution of 583 ps for the Rogowski probes. All the other CVD and Rogowski probes on the setup had similar transfer functions and bandwidths.

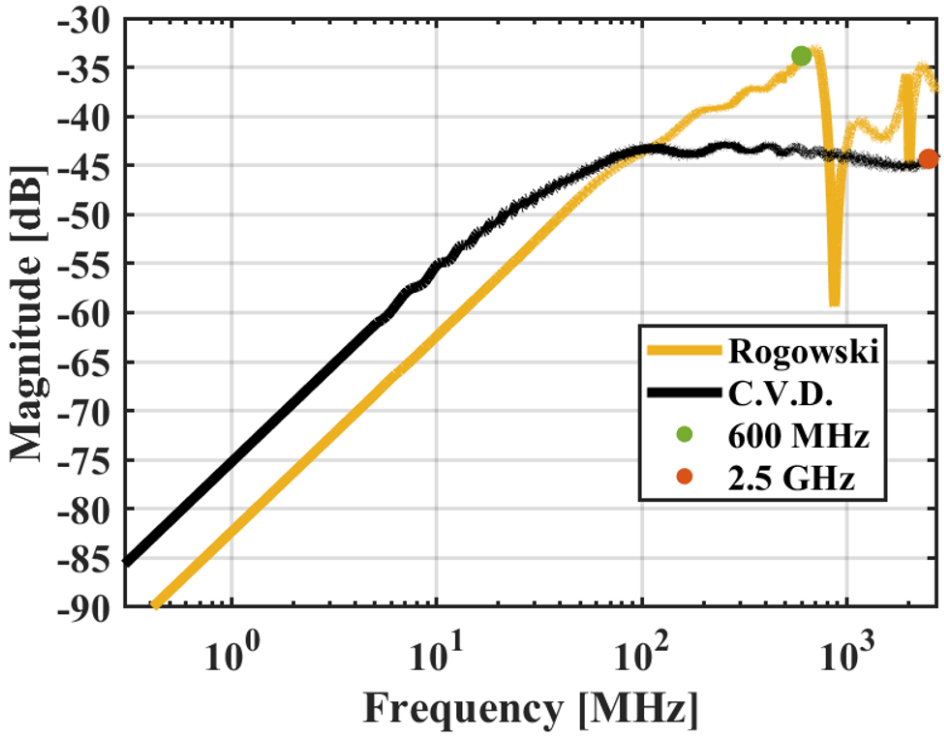

Figure 4. Measured transfer functions of the Rogowski and CVD probes. The usable frequency of each probe is 600 MHz for the Rogowski coil and 2.5 GHz for the CVD.

The transfer function of the diagnostic probes is used to calculate the input signal measured by the probes using discrete Fourier transform analysis. The oscilloscopes are in a Faraday cage some distance from the pressure chamber to reduce noise. All probes are connected to the oscilloscopes via 12.2-m RG223 cables. To account for the high-frequency losses of these cable lengths, the cable transfer function was measured on the VNA in situ, similar to other works [22,26].

2.3. Marx Generator Output

To isolate the effects of the gas within the spark gap, the consistency of the high-voltage pulse source is measured. An 8-stage Marx generator is used to generate the high voltage, HV, pulse in this setup. The Marx generator is charged to −38 kV and is arranged in an inverting configuration so the output pulse is positive. The Marx generator is pressurized to 304 kPa of lab air and is electrically triggered using a trigatron in the first stage electrode [27]. The output is captured using a CVD, as depicted in Figure 1.

The output voltage waveform of the Marx generator is shown in Figure 5. The maximum output voltage, risetime, and dV/dt are calculated for every shot. The Marx generator produces a 83.5 kV, 10 ns rise time excitation (6.8 kV/ns). The standard deviations in amplitude and risetime were observed to be 3% and 8%, respectively. However, due to losses in the 2121 HV cable spool, what reaches the cable is very similar in shape to the Marx generator output waveform but 10 kV lower in amplitude. All datasets in the report have similar Marx generator outputs. Based on the statistical deviation of the Marx generator, the breakdown electric field may vary anywhere between 3.3–16.1 kV/cm.

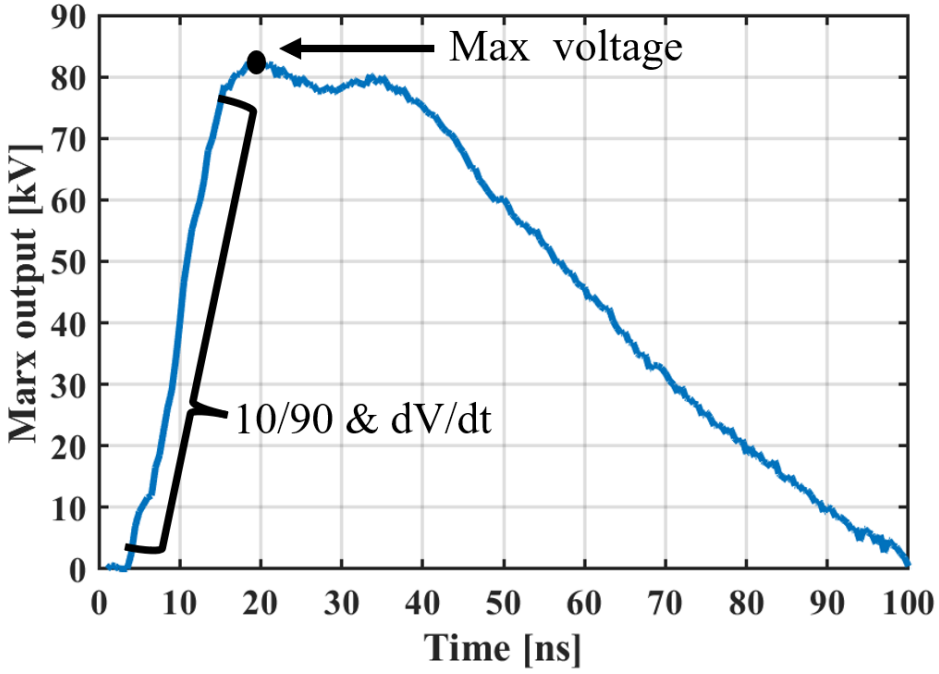

Figure 5. A sample waveform of the Marx generator output voltage. Three different attributes of the output waveform are measured to verify shot consistency; the risetime, the dV/dt, and the maximum voltage.

3. Results and Discussion

An example of a measured breakdown event in 203 kPa of 100% C_4F_7N is shown in Figure 6. Breakdown occurs when the gap voltage, V_{gap}, begins to collapse and is calculated according to Equation (2). V_{gap} is the differential voltage of the spark gap using the CVD probes. The signals V_H and V_L are temporally shifted by Δt to account for the electrical delay caused by the pressure chamber feedthroughs. The Δt used in the calculation is 0.5 ns. V_H is the input voltage on the high side of the setup. V_L is the voltage traveling down the load cable spools. I_H and I_L are the current measurements via the Rogowski probes. I_H captures the charging of the transmission line downstream from the Rogowski coil prior to breakdown. V_H measures the voltage increase at the spark gap. Once breakdown occurs V_H and V_L approach approximately the same voltage. The Rogowski measurements I_H and I_L help verify that no alternate breakdown paths formed. An alternate breakdown path is defined as an electrical breakdown not strictly across the two gap electrodes.

$$V_{gap}(t) = V_H(t - \Delta t) - V_L(t + \Delta t) \quad . \tag{2}$$

The nanosecond breakdown characteristics are primarily summarized by the maximum voltage across the gap, V_{max}, the time from voltage application to breakdown, τ_{br}, and the gap voltage collapse. The time to breakdown for this work is defined as the time it takes for V_{gap} to increase from 5 kV to its peak, see Figure 7.

The measured V_{gap} for SF_6 and C_4F_7N are given in Figure 8. As pressure increases, the voltage across the gap increases to 123 kV for SF_6 and 145 kV for C_4F_7N. Notably, the gap voltage measured in SF_6 showed a sharp oscillation in the falling edge, a feature that was not observed in C_4F_7N. LTSpice simulations revealed this to be caused by fall times of the gap voltage. SF_6 breaks down faster and has a shorter fall time than C_4F_7N, producing an oscillation in the gap voltage waveform because of the small impedance mismatches produced by the high voltage feedthroughs when transitioning from the DS-2121 cable to inside the pressure chamber. A noteworthy feature of the C_4F_7N data is the rounding off of the gap voltage at higher pressures such as 258 kPa, see Figure 8b, due to the Marx generators voltage output reaching its maximum.

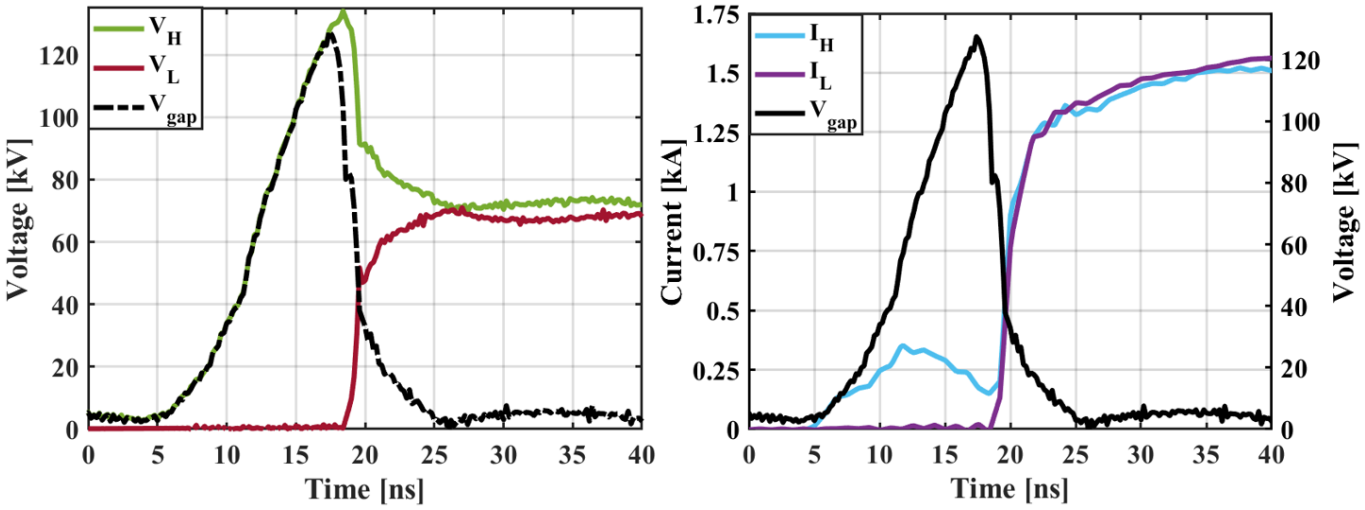

Figure 6. The experimentally measured waveforms V_H, V_L, I_H, I_L from their respective CVD and Rogowski probes. The subscript H denotes that the waveform is measured on the side of the spark gap connected to the Marx generator output. The subscript L denotes that the waveforms are measured on the load side of the setup. The data is from a pure C_4F_7N shot at 203 kPa. The gap voltage, V_{gap}, is calculated according to Equation (2) with a Δt of 0.5 ns to account for the delay of the chamber feedthroughs.

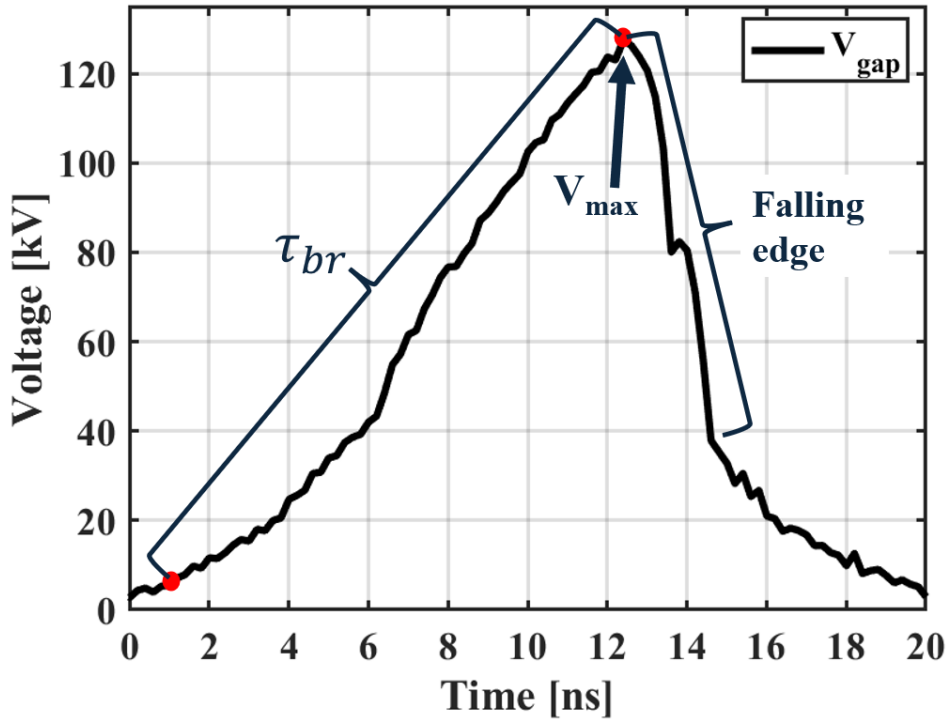

Figure 7. The gap voltage from a shot taken in pure C_4F_7N at 203 kPa. The time to breakdown, τ_{br}, is measured from 5 kV to the maximum voltage, V_{max}; the falling edge is when the insulating gas begins to form a plasma conducting channel between the electrodes.

The mean peak electric field versus pressure is plotted in Figure 9. The error bars represent 1 standard deviation across 30 shots for each dataset. The C_4F_7N dataset consists of 19 shots.

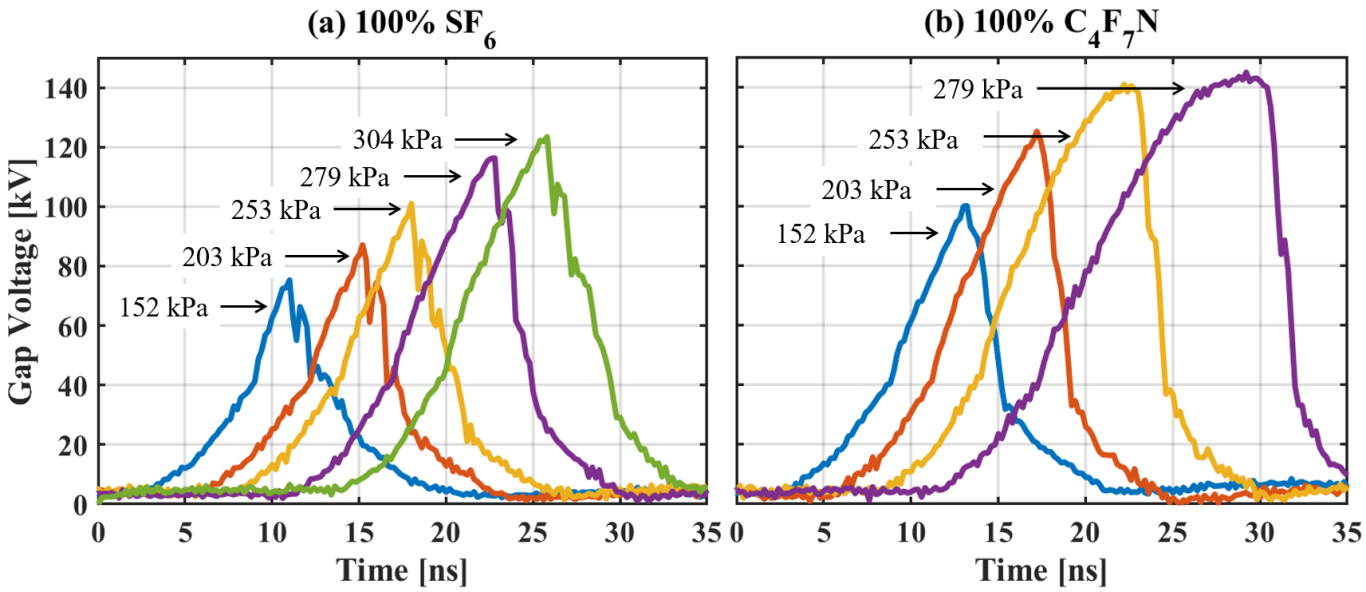

Figure 8. (**a**): Experimental gap voltage measured in pure SF_6 for varying gas pressure. (**b**): Gap voltage of pure C_4F_7N for varying gas pressures. The measured gap voltage for all the shots are temporally offset from one another for clarity. The 279 kPa gap voltage waveform for C_4F_7N begins to level off prior to breakdown due to the maximum output of the Marx generator being reached.

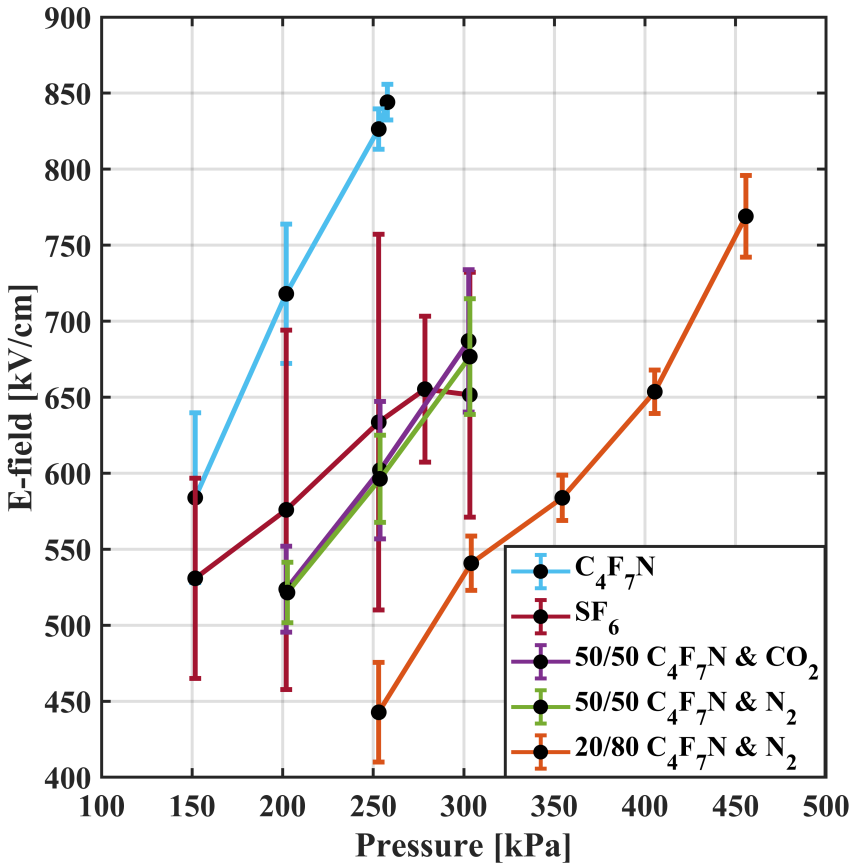

Figure 9. The mean peak electric field for pulsed breakdown versus pressure. The black dots are mean values, and the error bars are one standard deviation from the mean.

The 100% C_4F_7N data had the highest pulsed electric field hold-off of all the gases tested for 6.8 kV/ns signal. The standard deviation decreases dramatically at higher

pressures for pure C_4F_7N. As discussed previously, this is likely due to the rounding off of the gap voltage. The standard deviation of the Marx generator output was 2.7 kV, which translates to an electric field deviation of ±16.1 kV/cm. Thus, standard deviations that are more significant are presumed to originate from the gas between the spark gap. C_4F_7N overall, whether in pure or mixture form, has a lower standard deviation than SF_6. SF_6 also has measurable standard deviation in the electric field hold-off in other pulsed breakdown works [28,29]. In this experimental setup, SF_6 also appears to level off in electric field hold-off at higher pressure, which has been seen in other literature [30].

The 50% mixtures of C_4F_7N data show a similar performance to SF_6. This is in contrast to previous AC and DC testing, which only required 15–20% C_4F_7N mixtures to have a similar dielectric strength to SF_6 [4–6,31,32]. The 20/80 mixture of C_4F_7N and N_2 had the lowest hold-off performance versus pressure for a 6.8 kV/ns pulse. Interestingly, the standard deviation of the breakdown is still significantly lower compared to that of the SF_6, even approaching that of the Marx generator. At 405 kPa, the 20/80 mixture has the same mean hold-off electric field as 304 kPa SF_6 with a standard deviation limited by the Marx generator.

E/p versus p·τ_{br} graphs, see Figure 10, permit a pulsed breakdown comparison of various insulating gases [33]. However, the results are highly dependent on the dV/dt of the excitation pulse. For this experimental setup, these results apply to a HV pulse whose dV/dt is 6.8 kV/ns. For example, for a 15 ns, 102 kV peak pulse, an engineer may use a 3 mm gap with a 50/50 mixture of C_4F_7N with either N_2 or CO_2 at 152 kPa.

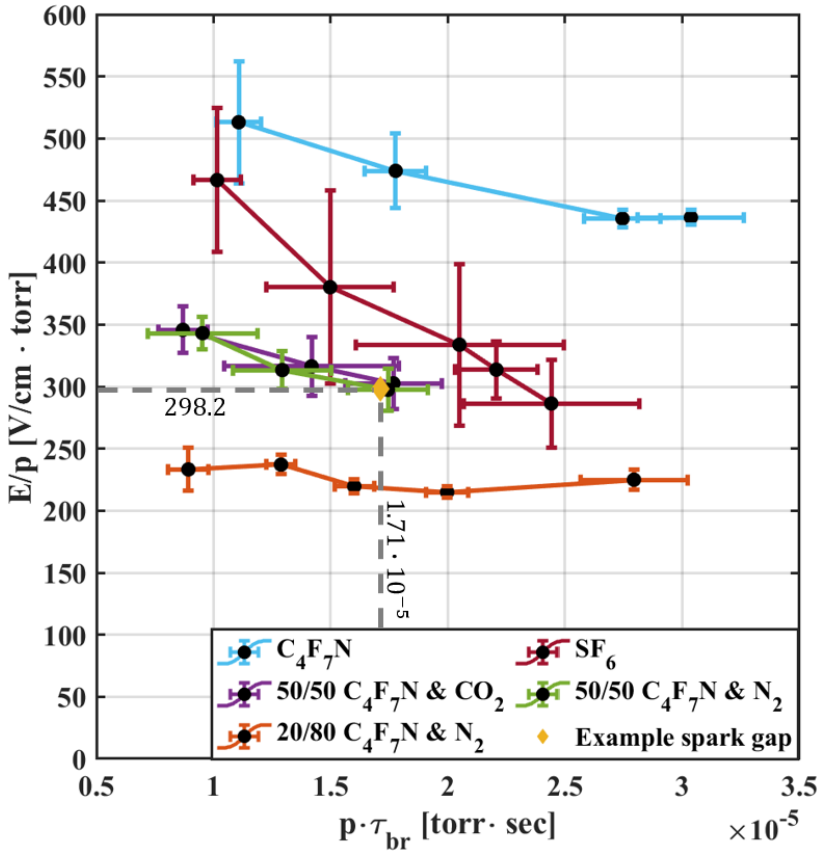

Figure 10. E/p versus p·τ_{br} of all the gases tested. The error bars are 1 standard deviation from the mean, black dot. Each data set averages 30–35 shots, except for 258 kPa C_4F_7N, which has only 19 shots. If an engineer wanted to design a spark gap to withstand a 6.8 kV/ns pulse for 15 ns, i.e., a peak voltage of 102 kV, they could use a 3 mm spark gap filled with a 50/50 mixture of C_4F_7N and CO_2 at 152 kPa. This results in a spark gap with an $E/p = 298.2$ V/(cm · torr) and a p·$\tau_{br} = 1.71 \cdot 10^{-5}$ torr · s, marked with the yellow diamond.

The standard deviation in τ_{br} is also represented in the p·τ_{br} axis of Figure 10. The time to breakdown will also have a natural standard deviation tied to Marx generator performance. Across the pressure ranges tested, 152 kPa to 456 kPa, this results in a minimum p·τ_{br} between $9.12 \cdot 10^{-7}$ torr·sec and $2.74 \cdot 10^{-6}$ torr·sec. SF_6 showed a wider variance compared to C_4F_7N and the associated mixtures.

Pure C_4F_7N has the highest hold-off performance of all the gases tested. Notably, the C_4F_7N datasets, mixtures included, exhibited a decrease in standard deviation in τ_{br} and peak electric field compared to the SF_6 datasets.

4. Conclusions

This paper reported the experimental characterization and comparison of the nanosecond pulsed breakdown behavior of SF_6, C_4F_7N, and C_4F_7N-based mixtures. C_4F_7N outperforms SF_6 in high voltage pulsed hold-off conditions experiencing a 6.8 kV/ns pulse. The 20/80 mixtures of C_4F_7N with N_2 did not match or exceed SF_6 performance in peak pulsed electric field hold-off, as shown in the previous DC and AC results [4–6,31,32]. Insulating gases, such as SF_6, in spark gaps show a wide variance in dielectric strength under pulsed electric fields [28–30]. The 50/50 mixtures of C_4F_7N with CO_2 and N_2 as buffer approached the performance of SF_6. C_4F_7N consistently showed less variation in breakdown characteristics, whether in pure or mixture form, compared to SF_6. The measured variation in breakdown performance of C_4F_7N at 253 kPa and 258 kPa can be attributed to the variance in the output pulse of the Marx generator. In future, larger datasets with a more consistent HV excitation source may be able to isolate the statistical variation in these pressure regimes. Notably, C_4F_7N has a lower vapor pressure and higher boiling point than SF_6; 294 kPa and −4.7 °C compared to 2108 kPa and −63.9 °C [3,34]. Thus, mixture and buffer gases are appealing to permit C_4F_7N to operate across large pressure and temperature regimes.

Other works have shown that C_4F_7N has many decomposition products, such as CN and CF_3, which occur with electron attachment or once the gas is fully ionized [3,9,12,35]. SF_6 tends to avoid these issues as long as impurities such as oxygen and water are kept low [36]. There are also long-term pulsed performance concerns of C_4F_7N, and its voltage holds off over time; some systems measured a 14% reduction in the dielectric strength of C_4F_7N and CO_2 mixtures after just 9 months [16]. C_4F_7N has a range of incompatible materials to be considered when designing HV systems [15–17,19]. These designs may have an increase in manufacturing costs, affect operational lifetimes, and require more research and design. Future research in development, deployment, cost, and environmental impact of C_4F_7N devices is still required for large-scale industrial applications.

Thus, C_4F_7N is not a simple drop-in replacement for SF_6 as more design considerations must be taken into account, such as lifetime, material compatibility, operating temperature and pressure regimes, and buffer gases. Under pulsed conditions, with relatively low shot numbers, C_4F_7N may be a suitable replacement for SF_6 but requires mixing ratios of 50% or more. Pure C_4F_7N also has a dielectric strength greater than SF_6 under pulsed conditions, permitting the design of more compact pulsed power systems. There is an ongoing search for alternatives to SF_6 as an insulating gas.

Author Contributions: Data collection and experiment construction, L.S., J.M. and L.B.; data processing, L.S.; writing, editing, data interpretation, L.S., J.S., A.N., J.D. and A.Y. All authors have read and agreed to the published version of the manuscript.

Funding: This work was performed under the auspices of the U.S. Department of Energy by Lawrence Livermore National Laboratory under Contract DE-AC52-07NA27344.

Data Availability Statement: The raw data supporting the conclusions of this article will be made available by the authors upon reasonable request (the raw data must be approved for release by sponsor).

Conflicts of Interest: The authors declare no conflicts of interest.The funders had no role in the design of the study; in the collection, analyses, or interpretation of data; in the writing of the manuscript; or in the decision to publish the results.

Abbreviations

The following abbreviations are used in this manuscript:

EPDM	Ethylene propylene diene monomer
CVD	Capacitive voltage divider
HV	High voltage
VNA	Vector network analyzer
AC	Alternating current
DC	Direct current

References

1. Li, X.; Zhao, H.; Murphy, A.B. SF6-alternative gases for application in gas-insulated switchgear. *J. Phys. D Appl. Phys.* **2018**, *51*, 153001. [CrossRef]
2. Owens, J.G. Greenhouse gas emission reductions through use of a sustainable alternative to SF 6. In Proceedings of the 2016 IEEE Electrical Insulation Conference (EIC), Montreal, QC, Canada, 19–22 June 2016; pp. 535–538.
3. Ahmed, R.; Abd Rahman, R.; Kamarudin, M.S.; Yousof, M.F.M.; binti Ahmad, H.; Salem, A.A. Feasibility of Fluoronitrile (C4F7N) as a Substitute to Sulphur Hexafluoride (SF 6) in Gas Insulated Application: A Review. In Proceedings of the 2022 IEEE International Conference on Power and Energy (PECon), Langkawi, Kedah, Malaysia, 5–6 December 2022; pp. 391–396.
4. Tu, Y.; Cheng, Y.; Wang, C.; Ai, X.; Zhou, F.; Chen, G. Insulation characteristics of fluoronitriles / CO2 gas mixture under DC electric field. *IEEE Trans. Dielectr. Electr. Insul.* **2018**, *25*, 1324–1331. [CrossRef]
5. Zhang, B.; Chen, L.; Li, X.; Guo, Z.; Pu, Y.; Tang, N. Evaluating the dielectric strength of promising SF6 alternatives by DFT calculations and DC breakdown tests. *IEEE Trans. Dielectr. Electr. Insul.* **2020**, *27*, 1187–1194. [CrossRef]
6. Hopf, A.; Britton, J.A.; Rossner, M.; Berger, F. Dielectric strength of SF6 substitutes, alternative insulation gases and PFC-gas-mixtures. In Proceedings of the 2017 IEEE Electrical Insulation Conference (EIC), Baltimore, MD, USA, 11–14 June 2017; pp. 209–212. [CrossRef]
7. Zhang, B.; Uzelac, N.; Cao, Y. Fluoronitrile/CO_2 mixture as an eco-friendly alternative to SF 6 for medium voltage switchgears. *IEEE Trans. Dielectr. Electr. Insul.* **2018**, *25*, 1340–1350. [CrossRef]
8. Zhang, T.; Zhou, W.; Zheng, Y.; Yu, J. Insulation properties of C4F7N/CO2 mixtures under non-uniform electric field. *IEEE Trans. Dielectr. Electr. Insul.* **2019**, *26*, 1747–1754. [CrossRef]
9. Li, Y.; Zhang, X.; Xiao, S.; Chen, Q.; Tang, J.; Chen, D.; Wang, D. Decomposition properties of C4F7N/N2 gas mixture: An environmentally friendly gas to replace SF6. *Ind. Eng. Chem. Res.* **2018**, *57*, 5173–5182. [CrossRef]
10. Hösl, A.; Chachereau, A.; Pachin, J.; Franck, C.M. Identification of the discharge kinetics in the perfluoro-nitrile C4F7N with swarm and breakdown experiments. *J. Phys. D Appl. Phys.* **2019**, *52*, 235201. [CrossRef]
11. Chachereau, A.; Hösl, A.; Franck, C.M. Electrical insulation properties of the perfluoronitrile C4F7N. *J. Phys. D Appl. Phys.* **2018**, *51*, 495201. [CrossRef]
12. Flynn, M.; Agan, J.; Neuber, A.; Stephens, J. Generation and optimization of cross-sections for electron-C4F7N collisions. *J. Phys. D Appl. Phys.* **2023**, *56*, 485207. [CrossRef]
13. Zhang, B.; Hao, M.; Yao, Y.; Xiong, J.; Li, X.; Murphy, A.B.; Sinha, N.; Antony, B.; Ambalampitiya, H.B. Determination and assessment of a complete and self-consistent electron-neutral collision cross-section set for the C4F7N molecule. *J. Phys. D Appl. Phys.* **2023**, *56*, 134001. [CrossRef]
14. Ovad, T.; Sapunar, M.; Sršeň, Š.; Slavíček, P.; Mašín, Z.; Jones, N.C.; Hoffmann, S.V.; Ranković, M.; Fedor, J. Excitation and fragmentation of the dielectric gas C4F7N: Electrons vs. photons. *J. Chem. Phys.* **2023**, *158*, 014303. [CrossRef] [PubMed]
15. Zhang, X.; Wu, P.; Cheng, L.; Liang, S. Compatibility and interaction mechanism between EPDM rubber and a SF6 alternative gas—C4F7N/CO2/O2. *ACS Omega* **2021**, *6*, 13293–13299. [CrossRef] [PubMed]
16. Gao, W.; Cao, Y.; Wang, Y.; Price, C.; Ronzello, J.; Uzelac, N.; Laso, A.; Tefferi, M.; Darko, K. Materials compatibility study of C 4 F 7 N/CO 2 gas mixture for medium-voltage switchgear. *IEEE Trans. Dielectr. Electr. Insul.* **2022**, *29*, 270–278. [CrossRef]
17. Li, Y.; Zhang, X.; Zhang, J.; Chen, Q.; Li, Y.; Xiao, S.; Cui, Z.; Tang, J. Thermal compatibility between perfluoroisobutyronitrile-CO 2 gas mixture with copper and aluminum switchgear. *IEEE Access* **2019**, *7*, 19792–19800. [CrossRef]
18. Li, Y.; Zhang, X.; Xiao, S.; Zhang, J.; Chen, D.; Cui, Z. Insight into the compatibility between C4F7N and silver: Experiment and theory. *J. Phys. Chem. Solids* **2019**, *126*, 105–111. [CrossRef]
19. Huang, Q.; Wang, Y.; Liu, J.; Zhang, Y.; Zeng, L. Study on the compatibility of gas adsorbents used in a new insulating gas mixture C4F7N/CO2. *Processes* **2019**, *7*, 698. [CrossRef]
20. Pellinen, D.G.; Di Capua, M.S.; Sampayan, S.E.; Gerbracht, H.; Wang, M. Rogowski coil for measuring fast, high-level pulsed currents. *Rev. Sci. Instrum.* **1980**, *51*, 1535–1540. [CrossRef]
21. van Oorschot, J.J.; Huiskamp, T. Rogowski and D-Dot Sensors for Nanosecond High-Voltage and High-Current Pulse Measurements in Impedance-Matched Pulse Generators. *IEEE Trans. Plasma Sci.* **2023**, *51*, 1107–1116. [CrossRef]
22. Huiskamp, T.; Beckers, F.J.C.M.; van Heesch, E.J.M.; Pemen, A.J.M. B-Dot and D-Dot Sensors for (Sub)Nanosecond High-Voltage and High-Current Pulse Measurements. *IEEE Sens. J.* **2016**, *16*, 3792–3801. [CrossRef]

23. Dubickas, V.; Edin, H. High-Frequency Model of the Rogowski Coil With a Small Number of Turns. *IEEE Trans. Instrum. Meas.* **2007**, *56*, 2284–2288. [CrossRef]
24. Wei, B.; Liu, H.; Liang, J.; Yuan, J.; Xie, W. A novel broadband capacitor voltage divider for measurement of ultrafast square high voltage pulse transmitted in transmission line. *AIP Adv.* **2020**, *10*, 045035. [CrossRef]
25. Ryu, J.; Kwon, H.O.; Park, S.H.; Yim, D.W. A Square Patch Capacitive Voltage Divider for Measuring High-Voltage Ultrawideband Pulses in a Coaxial Pulse Forming Line. *IEEE Trans. Instrum. Meas.* **2016**, *65*, 680–684. [CrossRef]
26. Stephens, J.; Wright, T.; Saheb, D.; Silvestre, L.; Hendricks, W.; Black, N.; Mankowski, J.; Dickens, J.; Neuber, A.; Schrock, E.; et al. Experimental Characterization of a Genetic Algorithm-Optimized Nonlinear Transmission Line for High Power RF Generation. *IEEE Trans. Microw. Theory Tech.* **2024**, 1–8. [CrossRef]
27. Williams, P.; Peterkin, F. Triggering in trigatron spark gaps: A fundamental study. *J. Appl. Phys.* **1989**, *66*, 4163–4175. [CrossRef]
28. Mankowski, J.; Dickens, J.; Kristiansen, M. High voltage subnanosecond breakdown. *IEEE Trans. Plasma Sci.* **1998**, *26*, 874–881. [CrossRef]
29. Ryan, H.; Watson, W.; Dale, S.; Tedford, D.; Kurimoto, A.; Banford, H.; Hampton, B. Factors affecting the insulation strength of SF6 filled systems. *CIGRE* **1976**, *15*. Available online: https://www.e-cigre.org/publications/detail/15-02-1976-factors-affecting-the-insulation-strength-of-sf6-filled-systems.html (accessed on 26 November 2024). .
30. Malik, N.H.; Qureshi, A.H. A Review of Electrical Breakdown in Mixtures of SF6 and Other Gases. *IEEE Trans. Electr. Insul.* **1979**, *EI-14*, 1–13. [CrossRef]
31. Li, Y.; Zhang, X.; Zhang, J.; Fu, M.; Zhuo, R.; Luo, Y.; Chen, D.; Xiao, S. Experimental study on the partial discharge and AC breakdown properties of C4F7N/CO2 mixture. *High Volt.* **2019**, *4*, 12–17. [CrossRef]
32. Hu, S.; Zheng, Y.; Wang, L.; Zhou, W.; Yu, J.; Qiu, R. AC breakdown characteristics of C 4 F 7 N/air mixture under different electric field structures. In Proceedings of the 2020 IEEE International Conference on High Voltage Engineering and Application (ICHVE), Beijing, China, 6–10 September 2020; pp. 1–4.
33. Felsenthal, P.; Proud, J.M. Nanosecond-Pulse Breakdown in Gases. *Phys. Rev.* **1965**, *139*, A1796–A1804. [CrossRef]
34. Owens, J.; Xiao, A.; Bonk, J.; DeLorme, M.; Zhang, A. Recent development of two alternative gases to SF6 for high voltage electrical power applications. *Energies* **2021**, *14*, 5051. [CrossRef]
35. Fu, Y.; Yang, A.; Wang, X.; Rong, M. Theoretical study of the decomposition mechanism of C4F7N. *J. Phys. D Appl. Phys.* **2019**, *52*, 245203. [CrossRef]
36. Chu, F.Y. SF6 Decomposition in Gas-Insulated Equipment. *IEEE Trans. Electr. Insul.* **1986**, *EI-21*, 693–725. [CrossRef]